Journal of Applied Physics ARTICLE scitation.org/journal/jap

Giant reversible stress-induced change of resistivity in Ni-Mn-In-Co alloys

Cite as: J. Appl. Phys. **125**, 195103 (2019); doi: 10.1063/1.5088233
Submitted: 9 January 2019 · Accepted: 25 April 2019 ·
Published Online: 20 May 2019

Sergiy Konoplyuk,[1,a)] Volodymyr Kokorin,[1] Alexey Mashirov,[2] Elvina Dilmieva,[2] and Andrei Dalinger[3]

AFFILIATIONS

[1]Institute of Magnetism of NASU and MESU, Vernadsky Blvd., Kyiv 03680, Ukraine
[2]Kotelnikov Institute of Radio Engineering and Electronics, Russian Academy of Sciences, Moscow 125009, Russia
[3]Institut für Werkstoffkunde (Materials Science), Leibnitz Universität Hannover, Garbsen, Germany

[a)]**Electronic mail:** ksm@imag.kiev.ua

ABSTRACT

$Ni_{43}Mn_{37.8}In_{12.2}Co_7$ and $Ni_{43}Mn_{37.65}In_{12.35}Co_7$ polycrystalline alloys were tested mechanically in uniaxial compression in order to determine the stress–strain response and accompanying changes of electrical resistivity. Compression of the specimen by 9% at room temperature resulted in a 250% increase of resistivity followed by almost full recovery to its predeformation level upon heating to 400 K. Microstructural observations revealed that giant reversible changes of electrical resistivity occurred due to stress-induced martensitic transformation and shape recovery of plastically deformed grains induced by heating.

I. INTRODUCTION

Metamagnetic Ni-Mn based shape memory alloys[1–5] demonstrate different effects related to the large changes of the physical properties accompanying isothermal martensitic transformation (MT). The latter can be assisted by a magnetic field or external mechanical stress and result in magnetocaloric[6–8] or barocaloric effects,[9,10] giant magnetoresistance,[11] etc. The majority of the studies devoted to these alloys was focused on the influence of external stimuli on the caloric properties, i.e., elastocaloric[12] and magnetocaloric effects. However, a variation of the electric and magnetic properties under mechanical stress is also practically applicable, in particular, in sensor technologies. In previous work,[13] a large reversible variation of the DC resistance (elastoresistive effect) under uniaxial stress was observed in Ni-Mn-In alloys. The most valuable outcome of this investigation was the low critical stress (0.62 MPa/K for $d\sigma/dT$), which is sufficient to bring about a stress-induced MT. This value is far lower than that observed earlier in superelastic materials[14–16] and results from a significant softening of the shear modulus in Heusler $L2_1$ phases at temperatures above the structural transition.[17] The large variation of the electrical resistivity in Ni-Mn-In alloys under compressive stress results from the more than twofold increase of its value as austenite transforms into martensite in the course of the thermally induced structural transformation. Given the brittleness of polycrystalline samples, only a small part of this effect can normally be exploited. Co doping to Ni-Mn-X family alloys improves their ductility and, hence, doped alloys can withstand higher mechanical stress. Moreover, the difference between the electrical resistance of the martensitic and austenitic phases induced by thermally activated MT increases in the case of Co addition.[18,19] This indicates a possibly higher elastoresistive effect, which is favorable for practical applications.

In this study, two Ni-Mn-In-Co alloys were investigated to characterize the influence of Co additions on the stress–strain response and the elastoresistive effect. The compositions of the alloys were chosen such as to result in superelastic behavior at room temperature.

II. EXPERIMENTAL DETAILS

Ingots were melted in an induction furnace under an argon atmosphere followed by homogenization at a temperature of 1223 K for 50 h. The compositions of the alloys were $Ni_{43}Mn_{37.8}In_{12.2}Co_7$ and $Ni_{43}Mn_{37.65}In_{12.35}Co_7$ (at. %). For compression testing, $2\times2\times4$ mm^3 pieces were cut from the ingots by electrical discharge machining. The samples were ground and polished to remove surface defects induced by machining.

In situ optical observations of the samples' surface during mechanical testing were performed using a Keyence VHX

1000D optical microscope with a VHZ 100 UR (100–1000 magnification) lens at room temperature. The samples were positioned between puncheons of a miniature mechanical load frame and compressed along their long geometrical axis, while the strain was measured along the same direction. The deformation rate was 0.1 μm/s.

The X-ray diffraction (XRD) measurements were performed using a PANalytical X'Pert PRO MPD diffractometer with Cu K_α radiation; then, the crystal structure was identified using the ICDD (International Center for Diffraction Data) database. Electrical resistance was measured by the conventional four terminal method using a Keithley Model 2182 nanovoltmeter with a Keithley Model 220 current source in a Delta measurements mode to exclude thermal EMF. The temperature dependence of the resistance was recorded at the heating and cooling rates of 5 K/min.

III. RESULTS AND DISCUSSION

As shown in Fig. 1, electrical resistance demonstrates a pronounced growth on cooling for both alloys in a small temperature interval below room temperature. Upon heating, the initial resistance value is fully restored. This behavior is a typical signature of MT similar to that of a Ni-Mn-In compound with a content of In lying between 10 and 20 at. %.[4] As follows from the ρ(T) curves in Fig. 1, the characteristic start and finish temperatures of the phase transitions were $A_S = 291$ K, $A_f = 310$ K, $M_S = 275$ K, and $M_f = 255$ K for $Ni_{43}Mn_{37.8}In_{12.2}Co_7$ and $A_S = 263$ K, $A_f = 283$ K, $M_S = 242$ K, and $M_f = 222$ K for $Ni_{43}Mn_{37.65}In_{12.35}Co_7$. They show a good accordance with characteristic temperatures determined from thermomagnetic curves for these compositions elsewhere.[7] As follows from that study, the martensitic phase has low magnetization even under high magnetic field, whereas the austenitic phase is ferromagnetic. This indicates that MT in the $Ni_{43}Mn_{37.8}In_{12.2}Co_7$ and $Ni_{43}Mn_{37.65}In_{12.35}Co_7$ alloys is metamagnetic.

In order to determine the crystal structure of the alloys studied, XRD analysis was employed. Since the alloys have close compositions and MT temperatures, only XRD measurements of the $Ni_{43}Mn_{37.9}In_{12.2}Co_7$ alloy were taken. The XRD pattern obtained in the temperature interval of the martensitic phase is shown in Fig. 2. Only reflections belonging to the martensitic monoclinic structure are seen in the pattern at a temperature of 120 K. This structure is a modulated one with a modulation period of 14 (14M), belongs to the P12/m1 space group, and has lattice parameters $a = 4.25(7)$ Å, $b = 5.85(5)$ Å, $c = 30.11(5)$ Å, and $\beta = 93.67°$. The lattice parameters of the austenite were not determined, because the PANalytical X'Pert PRO MPD diffractometer could not operate in the temperature interval of the austenitic phase. Nevertheless, the results of numerous structural investigations of Ni-Mn-In and Ni-Mn-In-Co alloys evidence that in a wide composition interval, including the compositions studied here, the austenite has a Heusler $L2_1$ structure at temperatures just above MT temperatures.

In contrast to many shape memory alloys, including ones with a Heusler structure,[20,21] which typically show a 15%–20% growth of electrical resistance in the course of MT, Ni-Mn-In-Co alloys undergo more than a fourfold increase of resistivity (Fig. 1), which cannot be explained simply by the appearance of twin boundaries in the martensitic phase.

Generally, in nonmagnetic alloys,[22] the difference in crystal symmetry and density of defects between martensite and austenite is responsible for the change of resistivity upon MT. In alloys that undergo metamagnetic transitions, a different magnetic ordering of low and high temperature phases results in an additional contribution to this change. The variation of magnetic properties at a metamagnetic transition influences electron density and scattering mechanisms. Thus, in FeRh,[23] the phase transition occurring between ferromagnetic and antiferromagnetic states drastically changes electron-spin scattering, while in

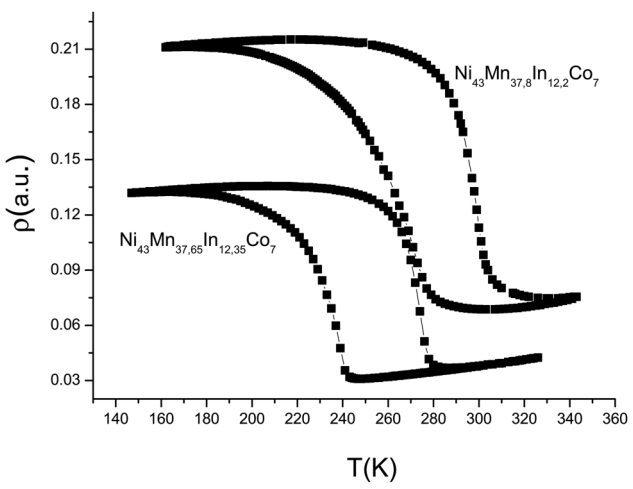

FIG. 1. Resistivity change upon MT in $Ni_{43}Mn_{37.8}In_{12.2}Co_7$ and $Ni_{43}Mn_{37.65}In_{12.35}Co_7$ alloys as monitored by DC resistometry.

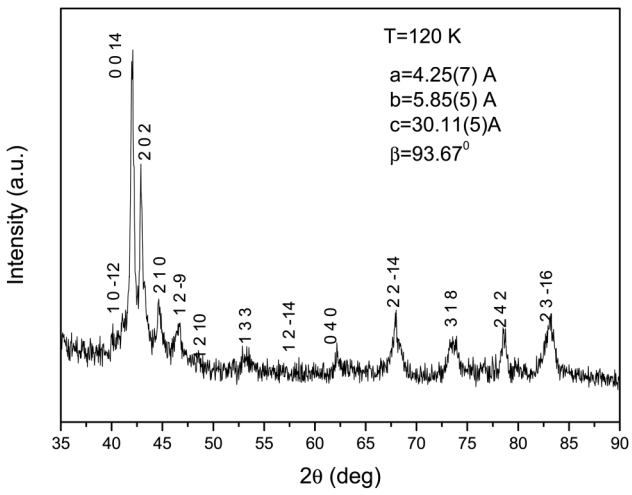

FIG. 2. The diffraction pattern of the $Ni_{43}Mn_{37.9}In_{12.2}Co_7$ alloy in the martensitic phase at T = 120 K.

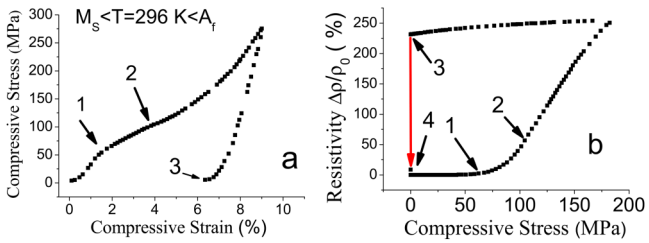

FIG. 3. Stress–strain (a) and stress–resistivity (b) responses of the $Ni_{43}Mn_{37.8}In_{12.2}Co_7$ alloy obtained upon straining up to 9%. The black arrows show the points corresponding to the same level of stress in both diagrams. The red arrow indicates the change of electrical resistance induced by heating to 400 K after sample unloading.

MnAs,[24] the metamagnetic transition takes place between ferromagnetic metal and paramagnetic insulator phases.

Measurements of the specific heat and thermal conductivity of Ni-Mn-In alloys[25] revealed that the large changes of electrical resistivity accompanying the forward and reverse MT are associated with the change of the free electron density at the Fermi level presumably due to the appearance and collapse of the superzone gap boundary.[26,27] According to these works, antiferromagnetic or other complex forms of magnetic ordering can introduce additional periodicities and, respectively, new Brillouin zone boundaries, which results in superzone gap formation on the Fermi surface and then a drop of resistivity in the process of a reverse MT to a ferromagnetic state. The series of experiments, including ferromagnetic resonance study[28] and observation of the exchange bias,[29] has confirmed that in the martensitic phase, competing ferromagnetic and antiferromagnetic interactions coexist in the Ni-Mn-In system. In contrast to Ni-Mn-In alloys, neutron diffraction and ferromagnetic resonance measurements performed on Ni-Mn-In-Co alloys[30,31] with compositions and martensitic temperatures close to the ones studied here have shown an absence of antiferromagnetic interactions and ordering in the martensitic phase. Nevertheless, one can see in Fig. 1 that the difference between the resistivity of the alloys in the martensitic and austenitic phases is even higher than that for the Ni-Mn-In alloys. Thus, a suggestion that antiferromagnetic ordering in the martensitic phase of Ni-Mn-In-Co alloys may be responsible for a large jump of resistivity upon MT is not supported by experimental evidence, and the reason for such behavior of resistivity is still not clearly understood. As seen in the stress–strain and resistivity–stress diagrams (Fig. 3), the application of mechanical stress triggers the transformation from austenite to martensite and results in changes in electrical resistance.

Deformation of the $Ni_{43}Mn_{37.8}In_{12.2}Co_7$ specimen under uniaxial compression occurs in several stages. The initial growth of stress up to a nominal strain of 1.5% corresponds to the elastic strain region. The electrical resistivity is essentially constant during this stage, implying that its variation caused by the contraction of the specimen is negligible. Beyond point 1 in the $\sigma(\epsilon)$ curve, where the curve becomes flatter, ρ begins to increase [Fig. 3(b)]. The microstructural observations (Fig. 4) provide evidence for the appearance of the first martensitic crystals at point 1, indicating that stress at this point corresponds to the critical stress σ_c of the stress-induced MT in the $Ni_{43}Mn_{37.8}In_{12.2}Co_7$ alloy. From Fig. 3, the critical stress is approximately 60 MPa. As deformation proceeds, the area covered by the martensitic plates increases.

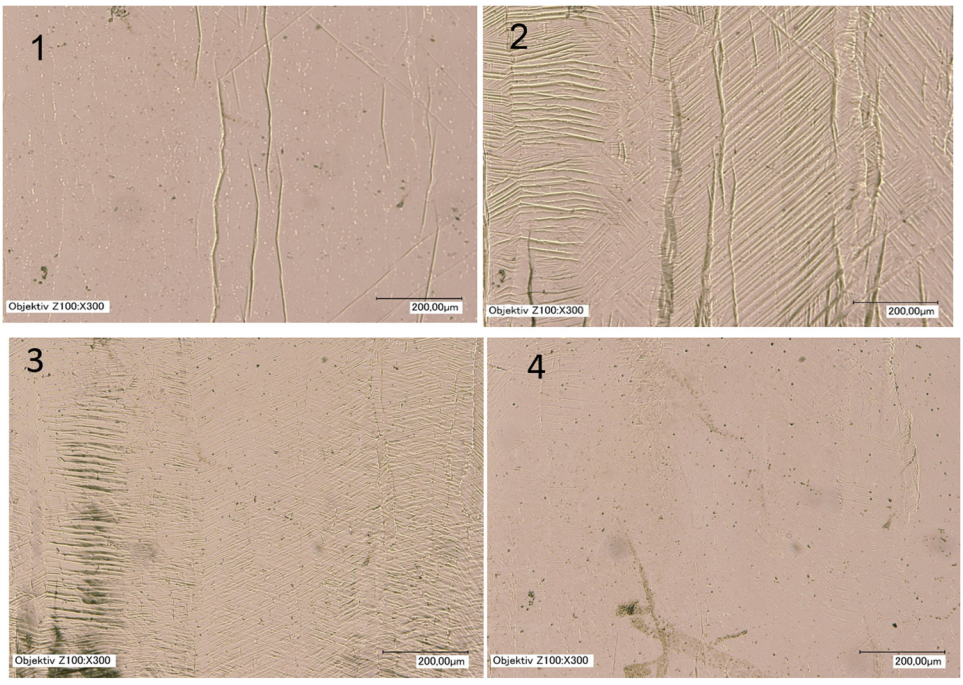

FIG. 4. Evolution of the surface during stress-induced martensitic transition caused by compression of the $Ni_{43}Mn_{37.8}In_{12.2}Co_7$ alloy. The numbers in the figures correspond to the points marked in the diagrams of Fig. 3.

At $\sigma \approx 85$ MPa, resistivity starts to grow sharply, while the formation and growth of martensite involves the bulk of the specimen (Fig. 4). In the micrograph (Fig. 4) corresponding to point 2, martensitic variants of different orientations are seen. In the first place, the formation of martensite occurs in the grains preferably orientated relative to the direction of compression according to their Schmid factor.

After attaining the maximal strain of 9% (Fig. 3), resistivity is 3.5 times as high as the initial value. In the course of the following unloading, the specimen length is not restored. Martensite plates are also retained on the surface (Fig. 4, image 3). The retained martensite is observed after unloading on the surface since the test temperature lies within the two-phase region. In addition, it is also preferentially present near local stress raisers. However, after heating the specimen up to 400 K, martensite almost disappears (Fig. 4, image 4) and resistivity is practically restored to its initial value. The reversible change of resistivity in the course of the stress-induced MT was about 250%.

In order to avoid residual martensite resulting from an incomplete reverse MT upon unloading, similar measurements were carried out on $Ni_{43}Mn_{37.65}In_{12.35}Co_7$, which has an austenite finish temperature of $A_f = 283$ K, i.e., below the test temperature. Uniaxial compression was performed first up to 7% and then up to 6% strain to determine the maximal possible deformation without cracking and the irreversible change of resistivity upon stress release. When deformation was limited to 6%, residual strain was below 2.5%. In this case, the initial stage of the stress–strain curve demonstrates a typical nearly linear character up to a strain of 3.5% and a stress of 150 MPa [Fig. 5(a)], where the steep initial growth of the compressive stress started to flatten out. This change of σ with ϵ is intrinsic to an alloy with a stress-induced MT. The critical stress σ_c of this MT is about 150 MPa, which is much higher than that for $Ni_{43}Mn_{37.8}In_{12.2}Co_7$. But if one compares $dT/d\sigma$ for these alloys, they are almost equal (350 K/GPa).

The difference in σ_c can be explained by the lower MT temperatures of $Ni_{43}Mn_{37.65}In_{12.35}Co_7$ ($M_S = 242$ K) with respect to the test temperature as compared to that of $Ni_{43}Mn_{37.8}In_{12.2}Co_7$ ($M_S = 275$ K). The critical stress σ_c coincides with the sharp growth of resistivity. This confirms that electric resistivity is a sensitive indicator of structural changes accompanying the MT.

The variation in resistivity during the MT at 6% strain is about 50%, while a strain of 7% results in an increase by 100%. Upon decreasing the stress, resistivity returns to its initial value, and for a maximum strain of 6%, almost full recovery of resistivity takes place. If the specimen is strained to 7%, only a part of the electrical resistance is restored after unloading, but, as in the case of $Ni_{43}Mn_{37.8}In_{12.2}Co_7$, heating to 400 K restores the resistivity to its original value.

Surface relief of the specimen after uniaxial compression and release of external stress is shown in Fig. 6. Both images [Figs. 6(a) and 6(b)] show the same area of the $Ni_{43}Mn_{37.65}In_{12.35}Co_7$ alloy before and after heating to 400 K. This area includes microcracks that had formed during the compression test, when the specimen was strained to 7%. The microcracks are mostly localized in the middle part of the specimen as was observed in the uniaxially compressed Ni-Mn-In alloy with identical shape and sizes.[32] The area near electric contacts at the ends of the samples of both compositions was free of any cracks even for strain of 9%.

As mentioned above, a stress-free MT is realized at temperatures below the test temperature for the $Ni_{43}Mn_{37.65}In_{12.35}Co_7$ alloy. This implies that martensite shown in Fig. 6 is a deformation-induced martensite, which is metastable at the test temperature and caused by the elevated stress level present near cracks after unloading. Microcracks appear in the boundaries between grains differently oriented with respect to the external stress applied to the specimen due to a different degree of deformation of these grains.

In the field without cracks [Fig. 6(c)], martensite is not seen on the surface of the sample. Upon heating to 400 K, the deformation-induced martensite gets into the temperature range of instability and most of it transforms back into austenite. This structural transition causes shape recovery of grains contiguous to the microcrack seen in Fig. 6(a) and, consequently, it closes [Fig. 6(b)]. The deformed surface areas restore their original shape owing to the reverse MT according to the mechanism of the shape memory effect. The closure of the microcracks occurs since they are intergranular, and as the deformation-induced martensite transforms into austenite upon heating to 400 K, plastically deformed grains gain the same shape as it was before compression (shape memory

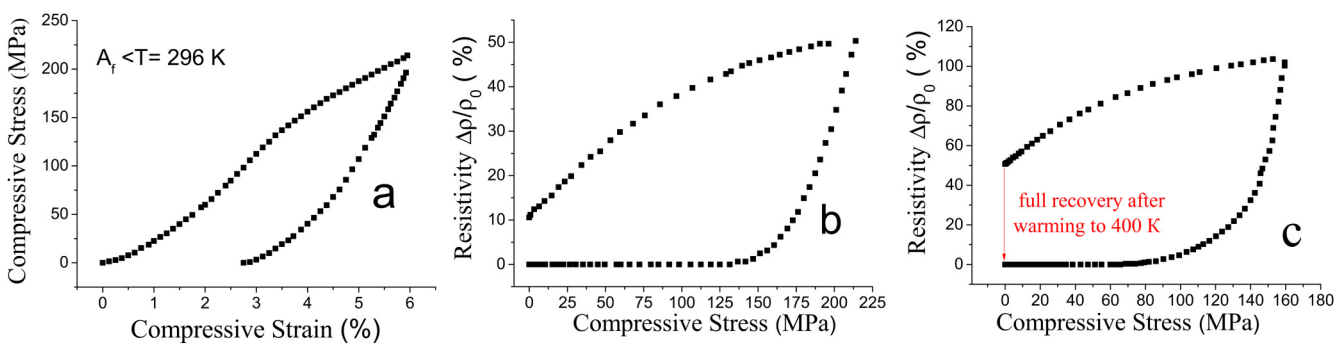

FIG. 5. Stress–strain (a) and stress–resistivity (b), (c) diagrams of the $Ni_{43}Mn_{37.65}In_{12.35}Co_7$ alloy.

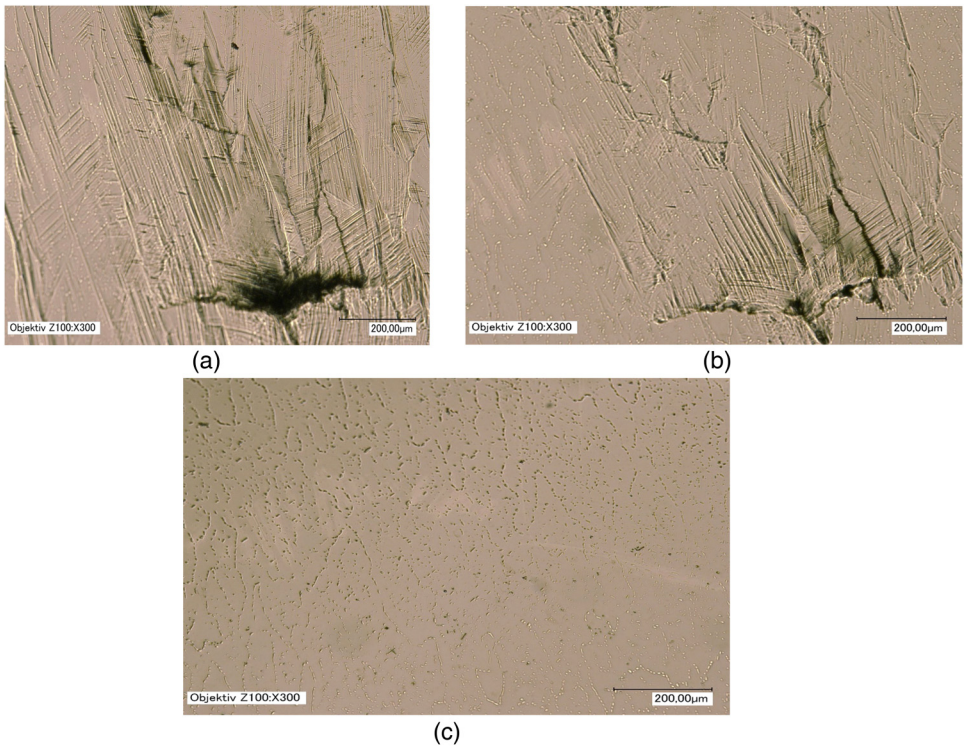

FIG. 6. Microstructural images of $Ni_{43}Mn_{37.65}In_{12.35}Co_7$ compressed by 7%: (a) after unloading in an area with a microcrack, (b) after the next heating up to 400 K in the same field, (c) after unloading in a field without cracks.

effect). Thus, they fill the same volume as it was before deformation and the cracks close up.

Simultaneously, electric resistance also recovers its value to the predeformation level [Fig. 5(c)]. Taking into account that heating is not able to change crack density, one can conclude that the deformation-induced martensite around the microcracks, rather than the microcracks themselves, is a source for residual resistivity. It follows from Fig. 5(c) that a significant part of the stress-induced resistivity variation (about 50%) originates in the deformation-induced martensite if the specimen is subjected to a 7% compressive strain. Thus, the martensite located in the plastically deformed regions around the microcracks is mostly retained after complete unloading, but in the process of heating to 400 K, its volume fraction drastically decreases, leading to a recovery of resistivity.

The results presented here demonstrate that $dT/d\sigma$ (350 K/GPa) for uniaxial compression significantly exceeds dT/dp for hydrostatic pressure. The latter was found to be about 50 K/GPa for the Ni-Co-Mn-In polycrystalline alloy.[33] A larger shift of MT temperatures under uniaxial compression than under a hydrostatic one is accounted for different mechanisms of deformation. Shear strain driven by uniaxial loading mainly contributes to lattice distortion occurring at MT. This mechanism of deformation requires a much lower stress when compared to that for hydrostatic pressure-induced volume changes to trigger MT. The values of $dT/d\sigma$ and dT/dp suggest good prospects for applications of elastocaloric, barocaloric effects, and giant stress-induced change of resistivity observed in Ni-Co-Mn-In alloys.

IV. CONCLUSION

Application of compressive stress to the Ni-Mn-In-Co alloys in the temperature interval of austenitic phase leads to a stress-induced MT accompanied by a huge 250% growth of electrical resistivity, which is almost fully restored to the initial value upon heating up to 400 K. Only partial recovery of the initial resistivity after the release of compressive stress is caused by residual martensite due to an incomplete reverse MT and (or) locally elevated stresses near microcracks. These microcraks are closed after heating to 400 K due to shape recovery of the deformed grains.

ACKNOWLEDGMENTS

The authors would like to thank Professor Maier (Institut für Werkstoffkunde, Leibnitz Universität Hannover) for great support and helpful discussion.

REFERENCES

[1]Y. Sutou, Y. Imano, N. Koeda, T. Omori, R. Kainuma, K. Ishida, and K. Oikawa, Appl. Phys. Lett. **85**, 4358 (2004).
[2]R. Kainuma, Y. Imano, W. Ito, Y. Sutou, H. Morito, S. Okamoto, O. Kitakami, K. Oikawa, A. Fujita, T. Kanomata, and K. Ishida, Nature **439**, 957 (2006).
[3]T. Krenke, M. Acet, E. Wassermann, X. Moya, L. Manosa, and A. Olanes, Phys. Rev. B **72**, 014412 (2005).
[4]T. Krenke, M. Acet, E. F. Wassermann, X. Moya, L. Manosa, and A. Planes, Phys. Rev. B **73**, 174413 (2006).

[5]S. Aksoy, M. Acet, E. F. Wassermann, T. Krenke, X. Moya, L. Maosa, A. Planes, and P. P. Deen, Philos. Mag. **89**, 2093 (2009).
[6]Z. D. Han, D. H. Wang, C. L. Zhang, S. L. Tang, B. X. Gu, and Y. W. Du, Appl. Phys. Lett. **89**, 182507 (2006).
[7]E. T. Dilmieva, Y. S. Koshkidko, A. P. Kamantsev, V. V. Koledov, A. V. Mashirov, V. G. Shavrov, and H. B. Grande, IEEE Trans. Magn. **53**, 1 (2017).
[8]J. Liu, T. Gottschall, K. P. Skokov, J. D. Moore, and O. Gutfleisch, Nat. Mater. **11**, 620 (2012).
[9]A. K. Nayak, K. G. Suresh, A. K. Nigam, A. A. Coelho, and S. Gama, J. Appl. Phys. **106**, 053901 (2009).
[10]L. Mañosa, D. González-Alonso, A. Planes, E. Bonnot, M. Barrio, J. L. Tamarit, S. Aksoy, and M. Acet, Nat. Mater. **9**, 478 (2010).
[11]S. Y. Yu, Z. H. Liu, G. D. Liu, J. L. Chen, Z. X. Cao, G. H. Guang, B. Zhang, and X. X. Zhang, Appl. Phys. Lett. **89**, 162503 (2006).
[12]B. Lu and J. Liu, Sci. Rep. **7**, 2084 (2017).
[13]V. V. Kokorin, S. M. Konoplyuk, A. Dalinger, S. Thurer, G. Gerstein, and H. J. Maier, Appl. Phys. Lett. **106**, 131908 (2015).
[14]C. H. Gonzalez, N. F. D. Quadros, C. J. D. Araújo, M. Morin, and G. Guénin, Mater. Res. **7**, 305 (2004).
[15]G. Airoldi, D. A. Lodi, and M. Pozzi, J. Phys. IV **7**(C5), 507 (1997).
[16]C. H. Gonzalez, M. Morin, and G. Guénin, J. Phys. IV **11**(PR8), 167 (2001).
[17]X. Moya, L. Mañosa, A. Planes, T. Krenke, M. Acet, M. Morin, J. L. Zarestky, and T. A. Lograsso, Phys. Rev. B **74**, 024109 (2006).
[18]W. Ito, K. Ito, R. Y. Umetsu, R. Kainuma, K. Koyama, K. Watanabe, A. Fujita, K. Oikawa, K. Ishida, and T. Kanomata, Appl. Phys. Lett. **92**, 021908 (2008).
[19]L. Chen, F. X. Hu, J. Wang, J. Shen, J. Zhang, J. R. Sun, B. G. Shen, J. H. Yin, and L. Q. Pan, J. Appl. Phys. **107**, 09A940 (2010).
[20]K. Otsuka, Y. Suzuki, K. Shimizu, Y. Sekiguchi, G. Tadaki, T. Honma, and S. Miyazaki, in *Shape Memory Alloys*, edited by H. Funakubo (Kyoto University, Kyoto, 1984).
[21]V. V. Kokorin, S. M. Konoplyuk, A. Dalinger, and H. J. Maier, J. Magn. Magn. Mater. **432**, 266 (2017).
[22]V. Antonucci, G. Faiella, M. Giordano, F. Mennella, and L. Nicolais, Thermochim. Acta **462**, 64 (2007).
[23]P. A. Algarabel, M. R. Ibarra, C. Marquina, A. del Moral, J. Galibert, M. Iqbal, and S. Askenazy, Appl. Phys. Lett. **66**, 3061 (1995).
[24]J. Mira, F. Rivadulla, J. Rivas, A. Fondado, T. Guidi, R. Caciuffo, F. Carsughi, P. G. Radaelli, and J. B. Goodenough, Phys. Rev. Lett. **90**, 097203 (2003).
[25]B. Zhang, X. X. Zhanga, S. Y. Yu, J. L. Chen, Z. X. Cao, and G. H. Wu, Appl. Phys. Lett. **91**, 012510 (2007).
[26]R. J. Elliott and F. A. Wedgwood, Proc. Phys. Soc. **81**, 846 (1963).
[27]N. V. Baranov and E. A. Barabanova, J. Alloys Compd. **219**, 139 (1995).
[28]S. Aksoy, O. Posth, M. Acet, R. Meckenstock, J. Lindner, M. Farle, and E. F. Wassermann, J. Phys. Conf. Ser. **200**, 092001 (2010).
[29]A. K. Pathak, M. Khan, B. R. Gautam, S. Stadler, I. Dubenko, and N. Ali, J. Magn. Magn. Mater. **231**, 963 (2009).
[30]A. S. B. Madiligama, P. Ari-Gur, V. G. Shavrov, V. V. Koledov, S. Calder, A. V. Mashirov, A. P. Kamantsev, E. T. Dilmieva, L. Gonzalez-Legarreta, and B. H. Grande, Smart Mater. Struct. **25**, 085013 (2016).
[31]K. Ollefs, C. Schöppner, I. Titov, R. Meckenstock, F. Wilhelm, A. Rogalev, J. Liu, O. Gutfleisch, M. Farle, H. Wende, and M. Acet, Phys. Rev. B **92**, 224429 (2015).
[32]V. V. Kokorin, S. M. Konoplyuk, A. Dalinger, S. Thürer, G. Gerstein, A. Mashirov, Y. P. Stetskiv, and H. J. Maier, MATEC Web Conf. **33**, 05007 (2015).
[33]T. Gottschall, K. P. Skokov, D. Benke, M. E. Gruner, and O. Gutfleisch, Phys. Rev. B **93**, 184431 (2016).